Reduced spatial spread of nodes in geometric network models improves topology associated with increased computational capabilities

Nicholas Christiansen[1] ✉, **Ioanna Sandvig**[1], **and Axel Sandvig**[1,2,3] ✉

[1]Department of Neuromedicine and Movement Science, Faculty of Medicine and Health Sciences, Norwegian University of Science and Technology (NTNU), Norway
[2]Department of Neurorehabilitation, Umeå University Hospital, Umeå, Sweden
[3]Department of Community Medicine and Rehabilitation, Umeå University, Sweden

Biological neural networks are characterized by short average path lengths, high clustering, and modular and hierarchical architectures. These complex network topologies strike a balance between local specialization and global synchronization via long-range connections, resulting in highly efficient communication. Here, we use a geometric network model with either an intermediate or a long-range connection probability to investigate the effects of wiring cost principles on network complexity for different spatial conformations. We find that both long-range and intermediate wiring probabilities only conform to small-world architectures for neurons in dense spatial clusters due to a decrease in wiring cost within clusters. Furthermore, both small-worldness and modularity were reduced in systems with long-range connections caused by a reduction in network clustering, allowing for novel insight into mechanisms underlying adaptive or maladaptive network alterations. Our findings corroborate previous work showing that both wiring probability and spatial distributions play a key role in neural network development.

networks | connectivity | small-world | spatial models

Correspondence: ***nicholas.christiansen@ntnu.no, axel.sandvig@ntnu.no***

Introduction

An intrinsic property of biological neurons during normal development is their ability to self-organize into functional complex network structures. These networks are formed through the establishment of connections between axons and dendrites, as neurites develop due to intrinsic growth programs, different external guidance cues and growth factors, and an interplay between activity-dependent and activity independent plasticity mechanisms (Onesto et al., 2021; Okujeni et al., 2017). The resulting networks are able to balance metabolic consumption with the cost of long-range connections, all while allowing for optimal capacity of information transfer (Laughlin, 2003; Beggs, 2008; Bullmore and Sporns, 2012). This confers the capability of larger dynamical changes in the global activity necessary for the complex computations performed by the brain as well as a protective effect on different types of perturbations to the network (Yamamoto et al., 2018; Kaiser, 2010; Pan and Sinha, 2007).

The study of these complex networks at different scales using concepts from network science and graph theory has gained increasing interest in recent years (Rubinov and Sporns, 2010; Khambhati et al., 2018), allowing for new insight into how network structure modulates activity (Massobrio et al., 2015; Okujeni and Egert, 2019a). This has revealed several topological hallmarks of these networks which are present across multiple scales, including their affinity for organizing into structures defined by a high degree of small-worldness, a hierarchical and modular organization, and a lack of characteristic scale (i.e. scale-free degree distributions) (Kaiser, 2010; Betzel et al., 2017; Goulas et al., 2019; Antonello et al., 2022). Though it is possible to model parts of the interactions leading to these topologies accurately, increasingly complex models have a higher computational cost. This has made such models challenging to utilize for larger network size. To compensate for this increased computational cost, it has been more common to reduce the complexity of network formation to that of a select few mean-field network models for modelling activity.

Among the most adopted network models we find the Erdós-Renyi (ER), Watts-Strogatz (WS) and Barabassi-Albert (BA) models (Erdos et al., 1960; Watts and Strogatz, 1998; Barabási et al., 1999). These models capture certain aspects of biological network structures at the expense of other important topological features. The ER model offers random networks reproducing the characteristic path length and clustering identified in biological networks, often used as a benchmark for measuring deviations from random networks (Betzel et al., 2017; Váša and Mišić, 2022). However, the ER model fails to reproduce the high degree of local and global clustering leading to small-worldness captured by the WS model, or skewed degree distribution of biological neural networks found in the BA model

(Klemm and Eguíluz, 2002). While using such models may provide useful insights, the functional outcomes of activity facilitated by the structural connectivity of neurons are intrinsically connected, and consideration should be taken when choosing which model to use (Massobrio et al., 2015). This becomes increasingly important when utilizing different network models for the study of functional outcomes from structural changes due to adaptive or maladaptive network responses, such as those occurring as healthy networks are subject to disease (Zhang et al., 2019; Akiyama et al., 2019; Garone et al., 2021), necessitating the need for better models.

To alleviate the lack of biological plausibility, the adoption of geometric network models as the basis for network generation has previously been proposed (Waxman, 1988; Kaiser and Hilgetag, 2004). Such models capture the underlying principles of neural network formation through an emphasis on the importance of spatial distributions of neurons and wiring cost principles on axon development (Chen et al., 2006; Onesto et al., 2017). In simplified terms, wiring cost principles propose that axon development can be reduced to a set of rules governed by an optimization to reduce global wiring length while maintaining a high level of computational efficiency combined with spatial constraints of component placement (Cherniak, 1994; Ahn et al., 2006; Chen et al., 2006; Hayward et al., 2023).

This proposed wiring cost optimization has been suggested to be aimed at reducing the metabolic consumption due to axon formation and maintenance over time, which is especially true for long-range connections, considered to be costly to both establish and maintain. To do so, self-organisation involves the clustering of neurons with similar roles, leading to highly interconnected modules of segregated function balanced by a few long-range connections to increase computational efficiency, resulting in a cost benefit trade-off on a macro- and microscale (Kaiser and Hilgetag, 2006; Goulas et al., 2019). These clusters arrange according to function, further supporting a balance of local integration and network wide synchrony (Cherniak, 1994; Hayward et al., 2023). Long-range connections, which may seem energetically unfavourable, have the role of facilitating a reduction in average path lengths, thereby increasing the speed of information transfer across the networks (Kaiser and Hilgetag, 2006). Previous work has shown that geometric network models can capture the structures of neural networks both in vivo (Kaiser and Hilgetag, 2004) and in vitro (Onesto et al., 2017). The use of these models therefore allows for the study of a variety of mechanisms in a computationally efficient manner, such as the effect of spatial clustering (Onesto et al., 2017; Gentile, 2024) or changes in network formation based on different wiring probability functions (Kaiser and Hilgetag, 2004; Gentile, 2021).

Despite the fact that geometric models have been shown to be tunable to small-world structures, the choice of tuning parameters and wiring probability function often does so at the cost of long range connections, as well as disregarding the assumption necessary for small-world network that the networks should be sparse (Ercsey-Ravasz et al., 2013). As a result, previous use of these models disregard the increased computational capacity and information transfer conferred to the network by the presence of these connections, focusing mainly on whether these models can be tuned to become small-world. On the contrary, the presence of long-range connections is often associated with an increased synchrony in networks (Arvin et al., 2022; Avramiea et al., 2022), balanced by separation into modules which facilitate larger dynamical ranges and response to external stimuli (Okujeni et al., 2017; Okujeni and Egert, 2019a,b; Yamamoto et al., 2018, 2023). Furthermore, the effect of adding long-range connectivity in relation to spatial clustering of neurons and their effect on modulation of network structures is not fully understood.

Here we adopt geometric network models to investigate the effects of simplified wiring cost principles combined with spatial constraints on network formation. We include two connection probability functions, one favoring short to intermediate connectivity (exponential), and one favoring short-range connectivity with a heavy tail (log-normal). Two aspects of interest were investigated, mainly how connections are recruited into the network for increasing network density, and how changes in spatial distributions alters the resulting networks following the differences in wiring probability. Through this, we aim to determine how the choice of connection preference may alter network hallmarks. By doing so, we gain novel insight into how differences in said connection preference influences the resulting network structures, which has proven challenging to determine using traditional methods for network generation.

Our findings suggests that the choice of connection probability function influences the resulting network parameters primarily below a certain network density, highlighting the importance of determining the sparsity of networks. The introduction of spatial constraints in low density networks increases hallmarks associate with optimal computational capacity, including larger degrees of modularity and small-worldness. Furthermore, we find that long-range connections without a sufficiently large cluster-

ing leads to a disruption of the network´s computational capabilities, through a decrease in modularity and small-worldness. This further emphasises the importance that not only the presence of long-range connections, but also a balance of long-range and local connectivity, is crucial for the formation of network structures associated with efficient computation and large dynamical ranges of activity. By including the presence of both long-range connections and spatial clustering of nodes in the systems, we offer new and novel insight into how these restrictions shape the resulting network properties.

Results

In the models used in this study, neurons are modeled as points termed nodes embedded in a space, whereas the connections between these nodes are meant to capture connection between nodes (i.e. physical connections such as axons or correlations in activity between regions or sub-units). We first initialized node placements before connecting each node using one of two probability functions.

Node placement. We initialized the systems by generating 100 different placements for each spatial clustering regime. One thousand nodes were placed in the unit square for each system, with all or a subset of nodes placed uniformly distributed in the area. Any remaining nodes were assigned an initially placed node to represent their frame of origin. To determine the distance from the chosen frame of origin, a power-law was used with $\alpha = 3/2$. The radial angles were chosen at random following a uniform probability. For clustered systems, either 200, 100, 50 or 20 nodes were initially placed, with the remaining nodes uniformly distributed around these. This resulted in increasing node densities around the initially placed nodes (Fig. 1). Cluster sizes were expected to have a mean size 5 (200), 10 (100), 20 (50) or 50 (20) nodes (initially placed nodes), corresponding to different regimes of clustering found in in vitro studies of neural networks (Okujeni and Egert, 2019b). Due to the distance from the initially placed node being determined by a power-law, most nodes were placed close to the initial node with a non-zero probability of a node being found at a large distance (Fig. 1c,e,g,i). The resulting systems had an increasing amount of unoccupied area as the distribution of nodes shifted to fewer and larger clusters (Fig. 1d,f,h,j).

To further determine how the spatial distribution changed local interactions for increased clustering, we estimated the probability density of the Euclidean distance to the nearest 1, 10 and 50 neighbors (Fig. 2). All systems with clustering showed a strong affinity for the nearest node to be found in close proximity, in contrast to the uniformly distributed systems (Fig. 2a,b). At a distance $d < 0.01$, the distributions were determined by the expected cluster size, and in all systems with clustering there was a peak at the smallest allowed distances from the initial node. This peak was more prominent for larger cluster sizes. For the systems with either 200 or 100 initially placed nodes, a bimodal distribution appeared for the 10 nearest neighbors (Fig. 2c,d). This bimodal distribution was also visible for systems with larger cluster sizes as the number of nearest neighbors considered was increased, suggesting that systems consisted of a densely packed core with interactions to distant nodes corresponding to a uniform distribution (Fig. 2e,f). When considering the 50 nearest neighbors, a bimodal distribution was visible in all systems containing clustering with the exception of the system with 20 nodes initially placed, likely due to the number of nearest neighbors considered corresponding with the expected cluster size.

Uniformly distributed nodes with increasing network density. To ascertain the range at which connections were added to the network for increasing network density (i.e increasing number of connections) and how this influenced network parameters depending on average degree $\langle k \rangle$, we generated networks with tuning parameters for connection probabilities chosen such that $\langle k \rangle$ varied from 20 to 500 for the uniformly distributed nodes. Networks were generated using both an exponential and a log-normal connection probability to determine the effect of choice of wiring probability function, referred to as the exponential and log-normal systems, respectively. The tuning parameters were manually chosen such that $\langle k \rangle$ for each system were comparable in the chosen range, with the same 20 uniform placements used to generate each network for both systems for increasing network density. This allowed us to determine how connections were recruited into the network for similar node placements for increasing $\langle k \rangle$, as well as assess how increasing network densities for different connection probability functions, favoring connections at different ranges, would affect common network parameters . A comparison of the connection probability functions for both functions tuned to $\langle k \rangle = 20$ can be seen in Appendix A.

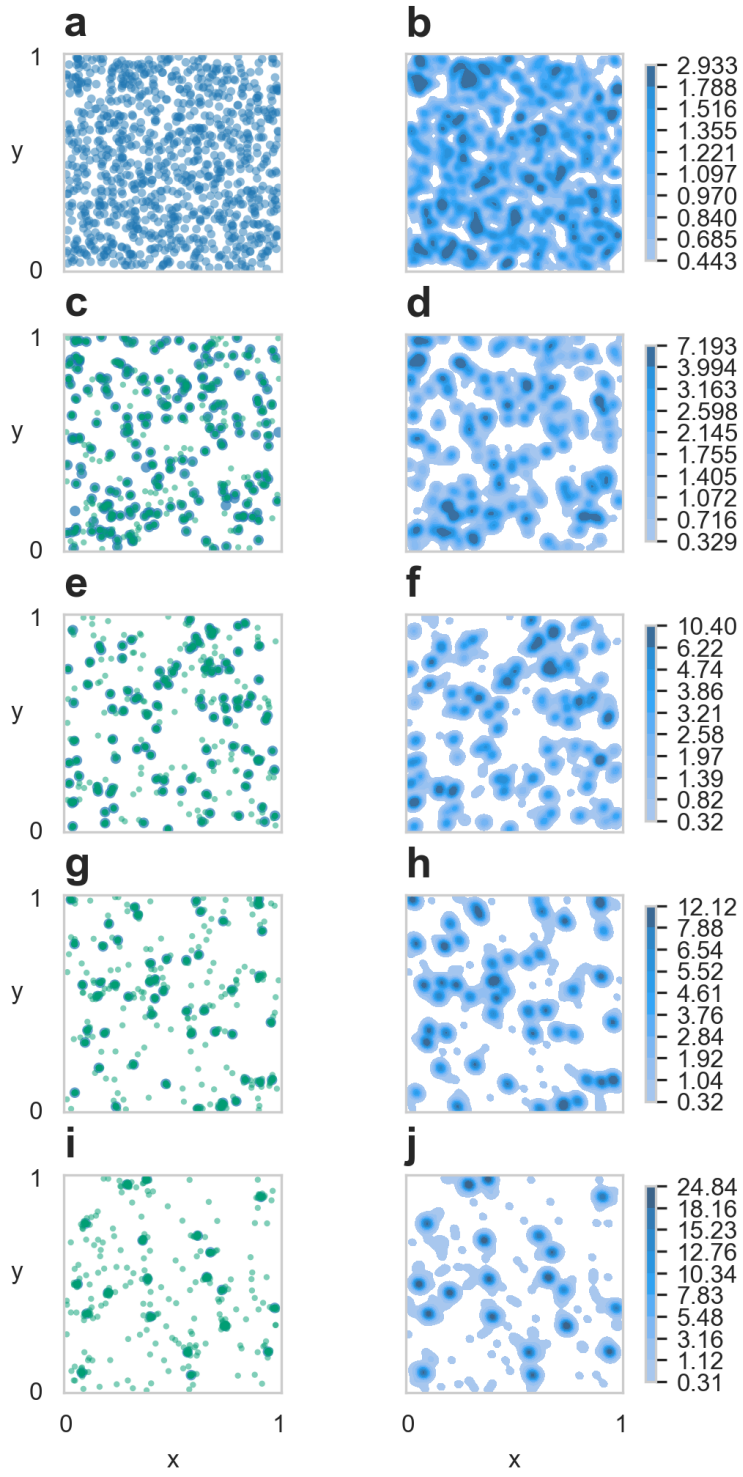

Fig. 1. Example of placements of nodes in the unit square for each spatial distribution with corresponding distribution density found using a Gaussian kernel. **(a)** The node distribution in the unit square for uniformly distributed nodes and **(b)** the corresponding density. **(c)**, **(e)**, **(g)** and **(i)** Node placements for increasing number of initially placed nodes with 200, 100, 50 and 20 nodes initially placed in the unit square, respectively. **(d)**, **(f)**, **(h)**, **(j)** Corresponding kernel densities for increasing cluster size. A total of 1000 nodes were placed in the unit square embedded on a torus for all distributions. Initially placed nodes colored blue and represented four times the size of the clustered nodes, colored green. In the density distributions, darker values of blue indicate stronger clustering. Note the difference in scale for the density distributions.

For low $\langle k \rangle$, the exponential systems displayed a preference for populating connections at short distances ($d < 0.25$), whereas long range connections were absent (Fig. 3a). Increasing $\langle k \rangle$ led to connections initially being added to the network at short and intermediate ranges, with only the denser networks having long-range connections (Fig. 3c). In contrast, the log-normal systems did not show

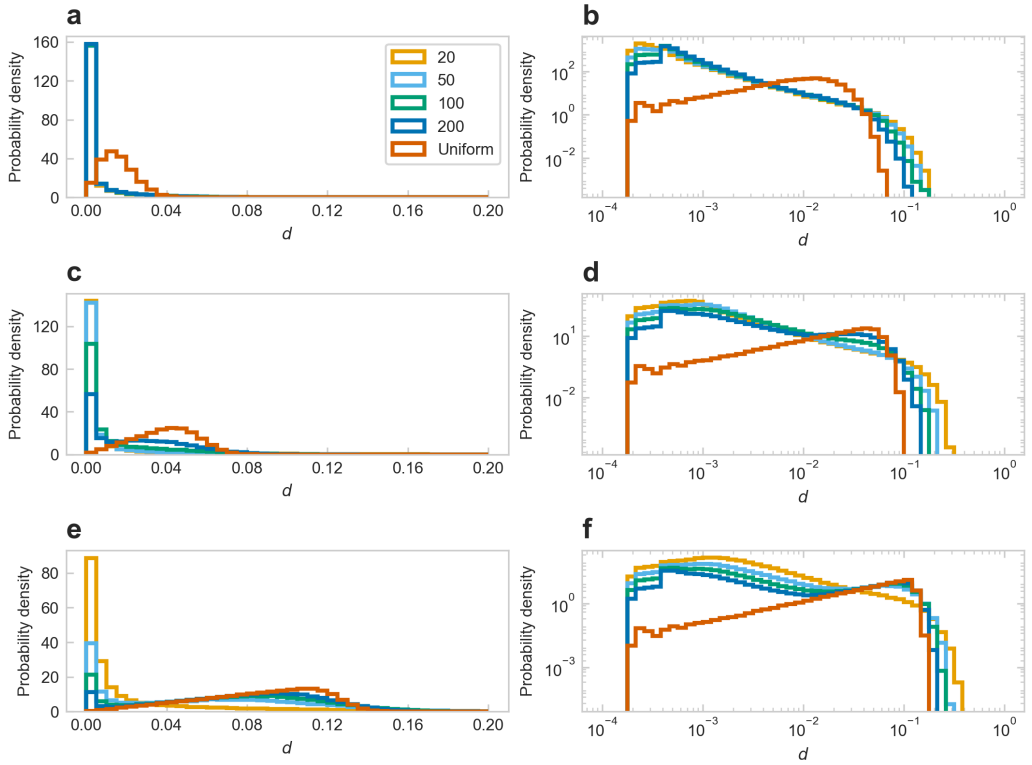

Fig. 2. Probability densities of euclidean distances to nearest neighbors for increasing number of neighbors. Probability density for the nearest one neighbor on a normal scale **(a)** and log scale using log binning **(b)**. Similarly, for 10 nearest neighbors **(c,d)** and 50 nearest neighbors **(e,f)**. As clustering increases the probability distributions shifts, increasing the probability of finding the closest node at a very short distance **(a, b)**. Increasing the number of closest neighbors considered results in a bimodal distribution for the intermediate clustering sizes (nodes clustered around 200, 100 and 50 nodes) in **c** and **e**, as the number of neighbors considered goes beyond the expected cluster sizes. For the largest clusters (20 initially placed nodes) there is a constant drop off and no bimodal distribution **(d,f)**, corresponding to the expected cluster size of 50 nodes per cluster. Each histogram shows the average value for the respective bin for 100 realizations of each configuration of a total of 1000 nodes. Legends are shared between figures. Error bars not shown due to small size.

the same strong preference for short range connections (Fig. 3b), with long range connections present even at low network densities (Fig. 3d). For these systems connections were more evenly distributed in the low and intermediate regions ($d < 0.50$) compared with the exponential systems for low network densities (Fig. 3a,b). With increasing $\langle k \rangle$ connections were added to intermediate to long ranges. For both systems there was a reduction in probability of finding connections at lower distances as network density increased, likely due to these connections being populated at low densities with a limited number of neighbors within this range (Fig. 2).

Long-range connections reduces path lengths and clustering. Tuning parameters showed that neither system followed an increase in $\langle k \rangle$ on a linear scale (Fig. 4a). At lower network densities, with $\langle k \rangle$ less than 200, the difference between the network parameters were more pronounced. In this range for the log-normal systems, both the average shortest path length $\langle d \rangle$ and network diameter d_{max} were lower than the exponential systems (Fig. 4b,c) as expected due to the presence of long-range connections at low $\langle k \rangle$ (Fig. 3c,d). In contrast, the clustering $\langle C \rangle$ was higher for the exponential systems compared to the log-normal systems (Fig. 4d). This suggests that the reduced presence of long-range connections combined with an increased preference for local connections in the exponential systems allows for more connectivity to occur locally resulting in increased $\langle C \rangle$. In opposition, the presence of long-range connections in the log-normal systems leads to an increase in available nodes to connect to, which is expected to reduce the number of connected neighbors before the network density reaches a certain threshold (Fig. 4d).
For $\langle k \rangle > 200$ both systems behave similarly, with values closely matched between systems (Fig. 4b-d), implying that the initial response for each system when adding connections changes as the network density increases. This is to be expected, as the probability of adding connections is higher for lower distances initially, as seen in Fig. 3. With an increasing number of connections added to the system, fewer nodes at lower ranges were likely to be available for establishing connections for any given node. In both systems $\langle d \rangle$ decreased and $\langle C \rangle$ increased accordingly, suggesting that the networks

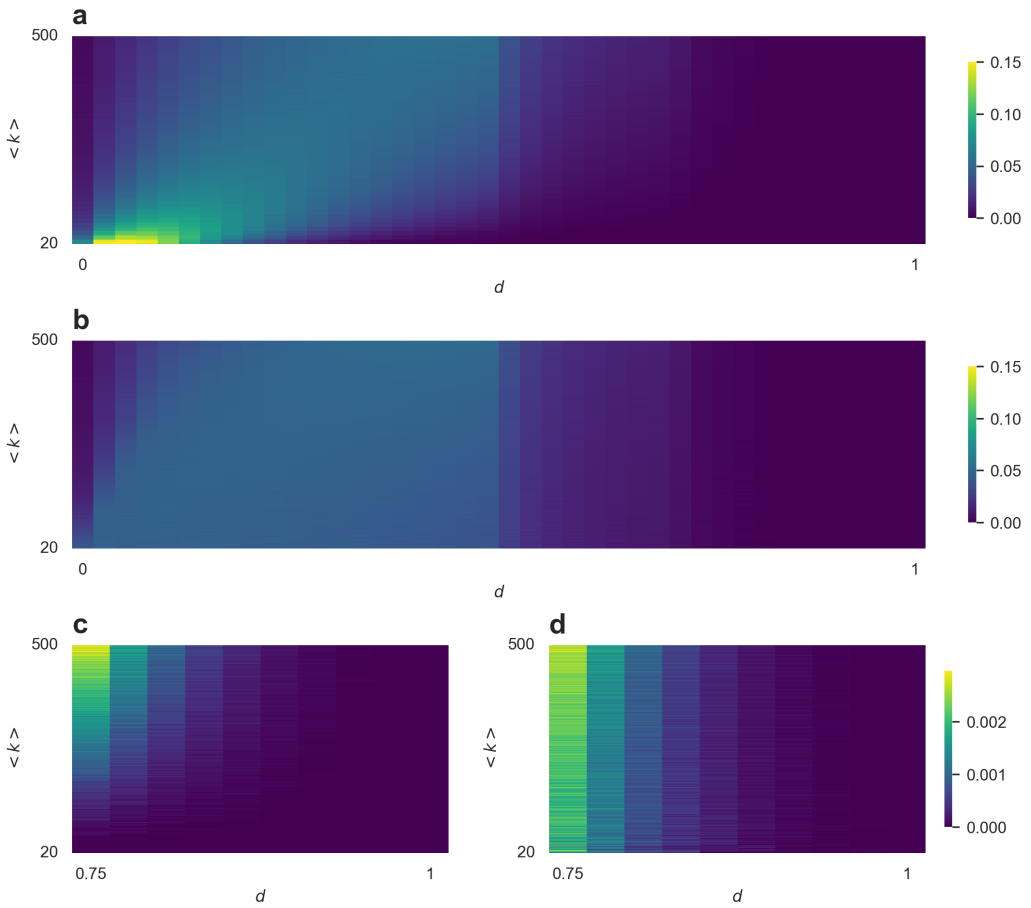

Fig. 3. Probability of finding a connection between two nodes at distance d for increasing average degree $\langle k \rangle$. **(a)** Probability of finding a connection at a given d for the exponential systems and **(c)** probability of finding a long range connection. **(b)** Probability of finding a connection at a given d for the log-normal systems and **(d)** probability of finding a long range connection. Darker colors indicate a lower probability and brighter colors indicate a stronger probability. Note the difference in scales between **a**,**b**, and **c**, **d**. All networks consist of $N = 1000$ nodes which are placed uniformly in the unit square embedded on a torus , with each $\langle k \rangle$ repeated for 20 instances for each system.

became well connected even for low network densities. We found that the impact on choice of connection probability function was more pronounced for sparse networks, resulting in standard network parameters being unable to discern between choices of connection probability as network density was increased. As such, sparse networks were more likely to be differentiated through the estimation of common network characteristics.

Clustering introduces highly connected nodes. Crucial to facilitating optimal neural activity, the neurons' physical placement in relation to each other determines wiring probability and onset and presence of sustained dynamical activity. To ascertain how increased cluster sizes (decreasing number of initially placed nodes) alter network hallmarks, we introduced clusters of nodes in the systems. For each cluster size, we generated networks using the same tuning parameters for both the exponential and log-normal systems, chosen such that $\langle k \rangle$ was approximately 20 for the uniform case in both.
The probability density function $P(k)$ of finding a node of given k showed that the introduction of clusters of densely packed neurons led to an increase in k in both systems (Fig. 5a,c). For the exponential systems, this led to a shift from nodes having approximately 20 connections in the uniformly distributed case, to larger variations with some nodes having more than 100 connections (Fig. 5a). In the log-normal systems the same tendency was visible, with the introduction of clustering resulting in increased k. However, for the log-normal systems, increasing the cluster size had less of an impact on the maximum k with $k < 110$ in all cases.
By calculating the probability $P(d)$ of finding a connection at distance d we found that both systems had a high affinity for short connections when clustering was introduced (Fig. 5b, d). At the longest distances the exponential systems had a stronger cutoff compared to the log-normal systems, with no $P(d)$ of finding connections beyond .9 and most connections falling in the range 0 to 0.5 (Fig. 5b).

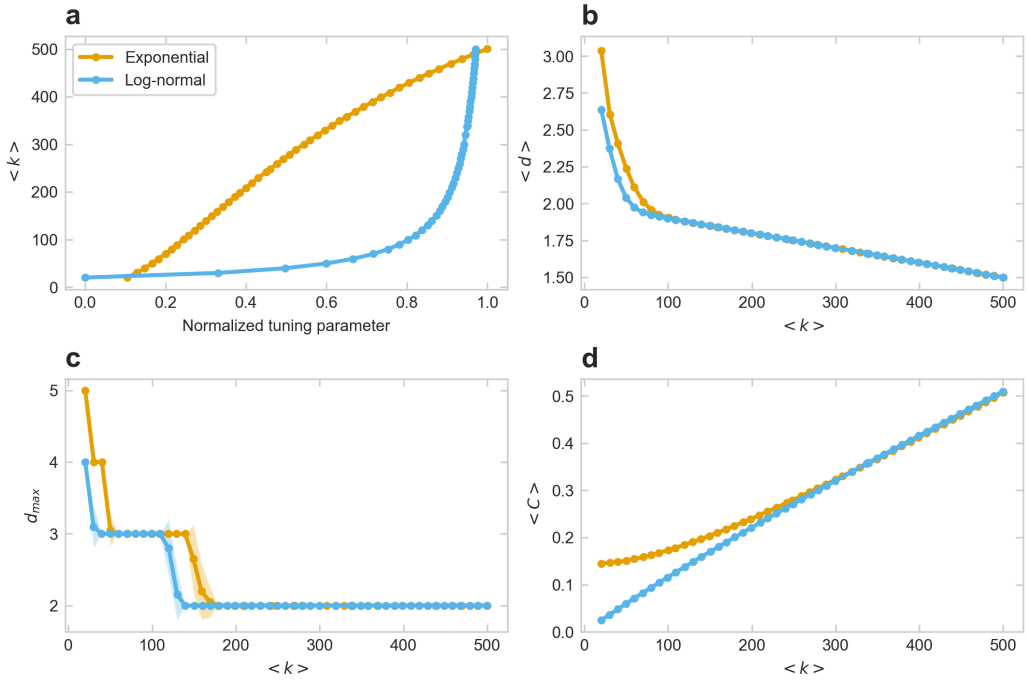

Fig. 4. Parameters describing network metrics for a uniform node distribution with increasing average degree $\langle k \rangle$. **(a)** Average degree $\langle k \rangle$ as a function of the normalized tuning parameter for the exponential (orange) and log-normal (blue) systems. The normalized exponential tuning parameter, used to determine the probability of a connection occurring between two nodes, is given by $\frac{\alpha}{\alpha_{max}}$. Similarly, the log-normal tuning parameters are found by the expression $1 - \frac{\sigma}{\sigma_{max}}$. For each wiring probability function, the tuning parameters were chosen such that $\langle k \rangle$ was evenly distributed on a linear scale between 20 and 500 for both systems. **(b)** Average shortest path $\langle d \rangle$, **(c)** network diameter d_{max} and **(d)** mean clustering $\langle C \rangle$ for increasing $\langle k \rangle$. All networks have $N = 1000$ nodes which are placed uniformly in the unit square embedded on a torus. Each value was determined from the mean of 20 instances of each respective system, with shaded areas showing the standard deviation in each figure. Legends shared between figures.

In contrast, the log-normal systems showed a sustained probability of long-range connections in the region 0.01 to 1 (Fig. 5d), as expected due to the heavy-tailed nature of the log-normal probability distribution. In both systems, $P(d)$ had a probability distribution at short ranges determined by an increased probability of interactions due to the increased number of neighbors as compared to the uniform node placements, with a distribution at $d > 0.01$ behaving similar to the the uniform distribution, albeit with a decreased probability due to the increased probability of connections occurring at lower distances.

Clustering promotes modularity and small-worldness. Through the introduction of clustering, the average number of connections increased with increasing cluster size (Fig. 6a). By reducing the inter-nodal distances by means of clustering, more connections were able to form between nodes due to the increased connection probability following the decrease in distance to an increasing number of neighbors within clusters (Fig. 2). These changes were comparable between both systems without additional tuning, suggesting that the changes brought on by the introduction of clustering were mostly due to local interactions. Compared to the log-normal systems, the exponential systems displayed a slight increase in $\langle k \rangle$ for the systems with the largest cluster sizes (initially placed nodes ≤ 50), including a larger variability. The average shortest distance $\langle d \rangle$ decreased in both systems with increasing cluster sizes (Fig. 6b), with the log-normal systems showing a lower $\langle d \rangle$ than the exponential systems for all spatial distributions as expected due to the presence of long-range connections. For both systems, increasing cluster size resulted in an increase in average clustering $\langle C \rangle$ for the resulting networks (Fig. 6c). However, for the exponential systems the introduction of spatial constraints led to an overall larger increase in $\langle C \rangle$ compared to the log-normal systems. The introduction of spatial clustering led to an increase in local connectivity, resulting in increased $\langle C \rangle$ in both systems, with a decrease in $\langle d \rangle$ due to reduced path lengths within clusters.

For low clustering densities, neither system showed any small-worldness when determining the small world propensity ϕ (Fig. 6d). Only in systems containing large clusters (50 or less nodes initially placed for the exponential systems and 20 for the log-normal systems) did we find networks which were considered to be small-world, suggesting that clustering in the spatial distributions of such net-

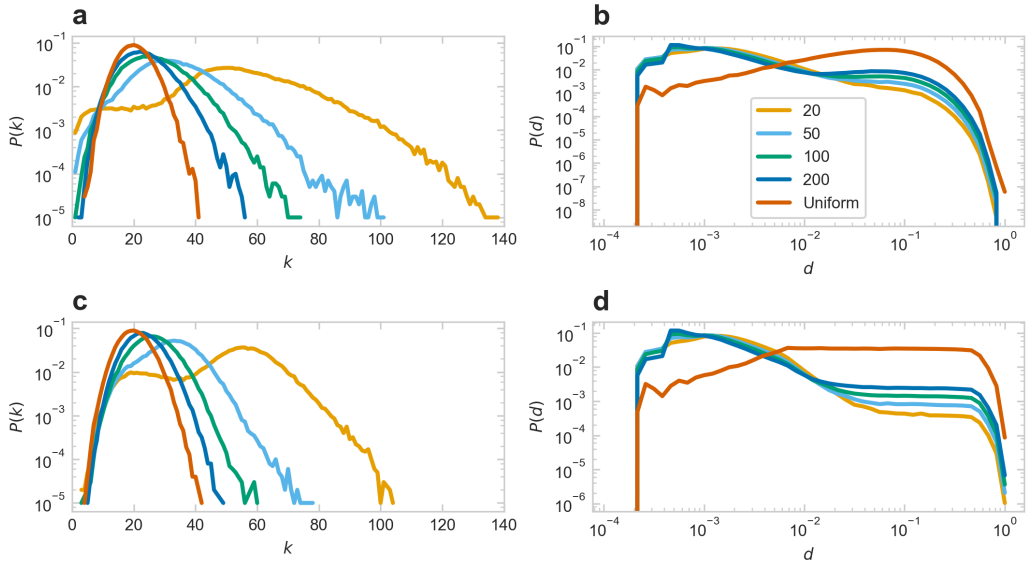

Fig. 5. Probability $P(k)$ of finding a node with a degree k, and the probability $P(d)$ of finding a connection at a distance d for different initial seeding numbers. **(a)** $P(k)$ as a function of k for the exponential and **(c)** log-normal systems for increasing cluster sizes. **(b)** Probability $P(d)$ of finding a connection between nodes at d for the for the exponential and log-normal systems, respectively. Note the difference in the y-axis. All networks have $N = 1000$ nodes placed in a unit square embedded on a torus. Nodes are placed clustered around 20, 50, 100 and 200 initially placed nodes or uniformly distributed. Each graph shows the average value for 100 realizations of each configuration. Legends shared between figures.

works is necessary to reach a sufficient balance between clustering and short average path to be termed as small-world. To determine whether the increased small-worldness was due to the increased number of connections of the exponential systems, we initiated systems with an average degree of 100 for the uniform system (Fig. B.1). We found that introducing more connections resulted in an overall reduction in ϕ, with no systems reaching the threshold for being considered small-world, suggesting that any difference between the two systems at $\langle k \rangle = 20$ is due to differences in how fast the connection probability function drops off at short distances. The log-normal systems have a steep initial decline with a sustained, albeit low, probability of making long-range connections, whereas the exponential systems favor short to intermediate connections. This affinity for local interactions results in a sufficiently larger $\langle C \rangle$ leading to small-worldness for the exponential systems. In opposition, for the log-normal systems the decreased $\langle d \rangle$ is not sufficient to facilitate an increase in ϕ, with the presence of long-range connections having a detrimental effect on $\langle C \rangle$. The same is seen for systems with larger $\langle k \rangle$, where connections are forced beyond the local vicinity of the respective node, resulting in an overall reduction of $\langle C \rangle$ due to the decreased probability of two neighbors sharing a connection at longer distances from the immediate node.

To ascertain how increased clustering would affect separation into communities, we determined network partitions for all systems using Q and Z modularity (Blondel et al., 2008; Newman and Girvan, 2004; Miyauchi and Kawase, 2016). For all spatial distributions, the exponential systems had a larger Q and Z modularity compared to the log-normal systems, with both systems displaying increasing modularity score with increasing clustering (Fig. 7 a, b). This difference was most pronounced when using Q modularity to establish the communities in the networks. For Q modularity, both systems showed an increase in modularity with increasing spatial clustering, whereas both systems displayed an increase in Z modularity followed by a slight decrease for the largest degree of clustering (Fig. 7b). For both modularity scores, the log-normal systems had a slightly larger number of communities in comparison to the exponential systems (Fig. 7c,d). Conversely, the exponential systems had comparatively larger mean cluster sizes (Fig. 7e,f).

For both Q and Z modularity, the exponential systems showed only slight changes in the number of communities with increasing spatial clustering accompanied by increased variability (Fig. 7c,d). In the exponential systems, a lower median number of communities were detected for all spatial distributions compared to the log-normal systems. For communities detected using Z modularity with $50 \leq$ nodes initially placed, the spread of the exponential systems increased to encompass the region spanned by the log-normal systems, but also had a slight decrease in the overall number of communities detected using Z modularity (Fig. 7c,d). In contrast, the log-normal systems showed an increase in community

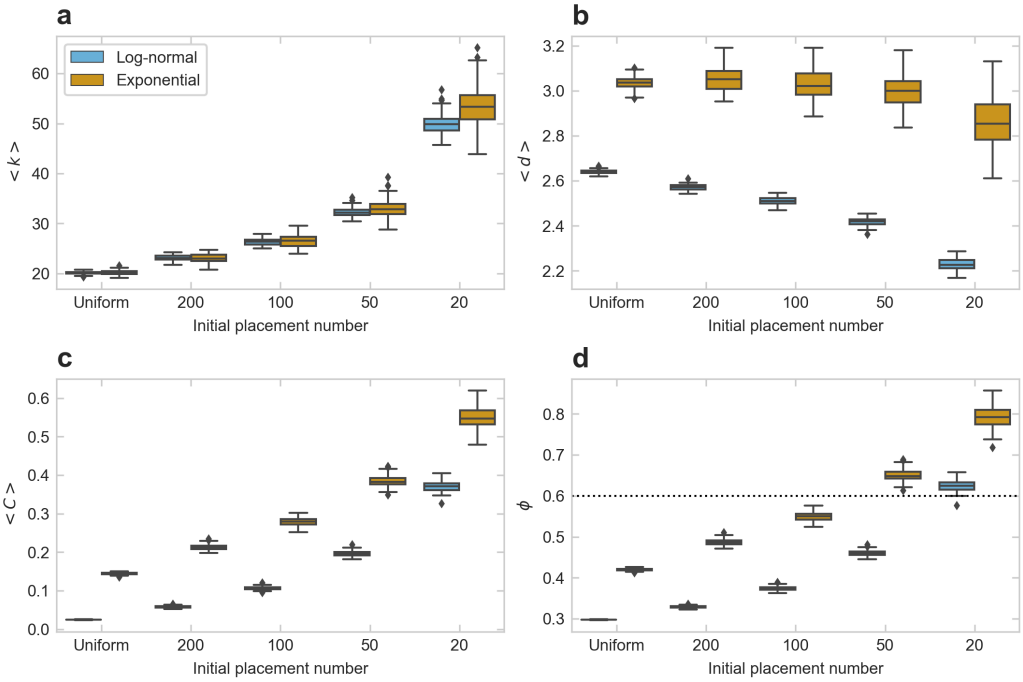

Fig. 6. Parameters describing common network characteristics for networks tuned to have a mean degree of 20 for the uniform distribution. **(a)** Average degree, $\langle k \rangle$, **(b)** average shortest distance, $\langle d \rangle$, **(c)** mean local clustering, $\langle C \rangle$ and **(d)** small-world propensity, ϕ, for the uniform node placement and increasing cluster size. The stippled line at 0.6 indicating threshold for small-worldness. All systems have $N = 1000$ nodes, and 100 instances are generated for each system. Each figure shows the box plot generated from of 100 realizations of each configuration. Legends shared between figures. Outliers denoted with diamonds.

sizes for Q modularity for increasing cluster sizes (Fig. 7c) with corresponding reduction in mean sizes (Fig. 7e). For Z modularity, the log-normal systems showed a decreasing number of communities as cluster sizes were increased (Fig. 7d) matched by a corresponding increase in cluster size (Fig. 7f). Although the exponential networks had both a larger Q and Z score, the partitioning into communities were less dependent on spatial clustering of the nodes, with only slight changes in the number of detected communities. Consequently, mean community sizes had correspondingly larger changes due to the inverse relation between the two. In contrast, the log-normal system exhibited more defined partitions with reduced spread between each realization of each configuration.

In hierarchical networks, the clustering $C(k)$ has been shown to depend on k, with $C(k)$ expected to follow a power law distribution (Ravasz and Barabási, 2003). Neither system displayed a strong affinity for heavy tailed distributions suggesting that $\langle C \rangle$ was not dependent on k. Even so, both systems had an increase in $C(k)$ for increasing cluster sizes. For exponential systems we found an increase in $C(k)$ following increased cluster sizes (Fig. 8a) as expected due to the increase in both $\langle k \rangle$ and $\langle C \rangle$ (Fig. 5a, Fig. 6c). Similarly, the increasing spatial clustering led to an increase in $C(k)$ for the log-normal system (Fig. 8b), yet with many nodes with large k showing a decreased $C(k)$ compared to the rest of the nodes. These nodes are likely close to large clusters, but not central, resulting in many connections to nodes that are not connected to other neighboring nodes, whereas the nodes with highest degree are likely to be central to clusters (i.e. initially placed nodes). These nodes have the most possible neighbors to connect to within proximity, with a high probability of these being connected as well.

Discussion

Here, we investigated how the choice of wiring probability function alters structural outcomes for networks with a variety of spatial constraints when generating networks using a simple geometric network approach, inspired by wiring cost principles. We find that adding spatial constraints in the form of clustering to the node placement of the geometric models improves network properties associated with improved functional outcomes in biological neural networks. The introduction of larger spatial clusters reduces the overall path length while also increasing network clustering, resulting in networks considered to be small-world. Our findings further corroborate the supposition that the small-worldness of these systems depends on the majority of connections being constrained within the respective cluster to which the node was initially placed, with a high probability of neighbors sharing connections. This

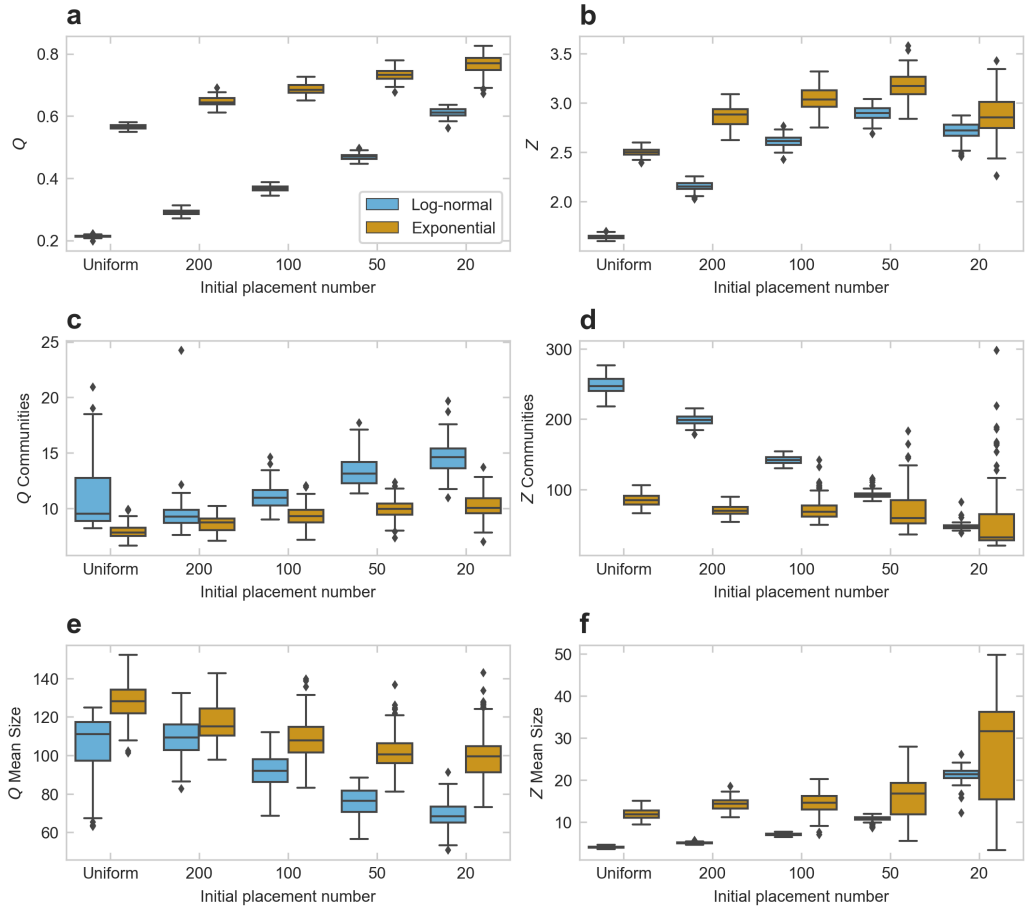

Fig. 7. Community detection using Q and Z modularity for graph partitioning. **(a)** Maximized modularity score for Q modularity and **(b)** and Z modularity. **(c)** Mean number of communities for each partition for Q modularity and **(d)** Z modularity. **(e)** Mean community size for partitions found using Q modularity and **(f)** Z modularity. Each box plot represents the values for 100 realizations of each configuration. Legends shared between figures. Outliers denoted with diamonds.

necessitates that the networks are sufficiently sparse to limit connections to within the local vicinity of the node, yet share a limited number of long-range connections to distant modules in the network to maintain computational efficiency.

The dynamical range and onset of activity in neuronal networks is inherently dependent on the structure of the network on which the activity propagates. This dependence has been seen both in computational studies and in in vitro models of neural networks (Massobrio et al., 2015; Yamamoto et al., 2018; Arvin et al., 2022). Through constraints on neuronal organization in the spatial domain, combined with wiring optimization, these networks have been shown to develop a high local clustering with long-range connections, resulting in a reduced number of steps necessary to traverse the network (Cherniak, 1994; Kaiser and Hilgetag, 2006; Hayward et al., 2023). The high degree of local clustering aids in increasing local feedback loops, whereas the network wide interconnectedness arising from long-range connections facilitate global interactions and synchrony in the networks, necessary for processing information (Markov et al., 2013; Okujeni et al., 2017; Arvin et al., 2022; Avramiea et al., 2022; Antonello et al., 2022). In the reductionist scheme using geometric network models, we find that structures associated with these dynamical ranges appear only as a consequence of high degrees of spatial clustering of nodes in the network, irrespective of the chosen wiring probability. With increasing clustering and decreasing inter-nodal distances, clustering and modularity increases, whereas the average path length is reduced. This indicates a shift towards a globally more segregated community structure with locally integrated nodes, suggesting that component placement plays an integral role in reducing the overall path length through local integration while also supporting formation of structures associated with diversified and sustained activity (Okujeni et al., 2017).

To our surprise, networks generated using either connection probability were only considered small-world when the nodes of the network were constrained to sufficiently large spatial clustering. In accordance with previous work, we found that networks generated using a heavy tailed connection

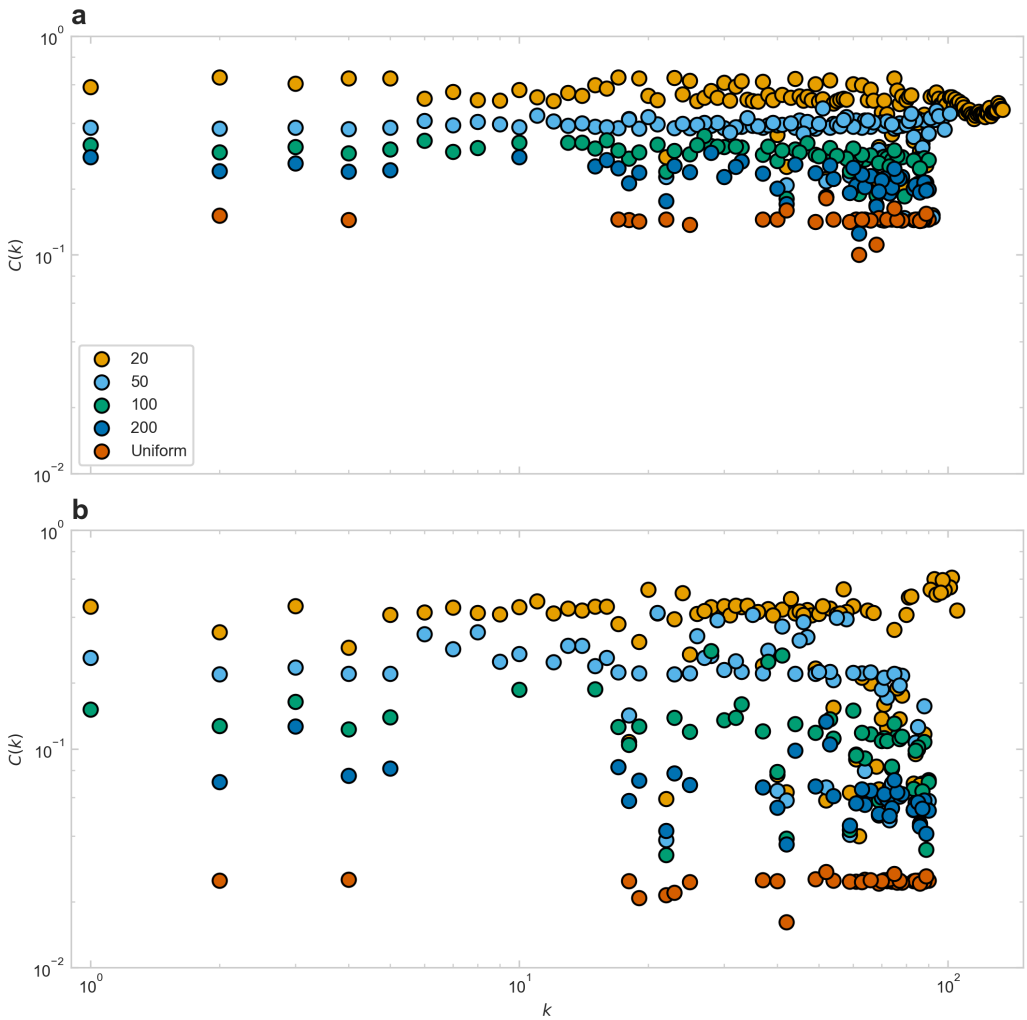

Fig. 8. Clustering $C(k)$ as a function of the degree k. **(a)** Dependence of $C(k)$ on k for the exponential systems for each spatial distribution. **(b)** Dependence of $C(k)$ on k for the log-normal systems for each spatial distribution. All values determined from the pooled mean $C(k)$ for each k consisting of 100 realizations of each conformation. Legends shared between figures.

probability, such as the log-normal connection probability, struggled to achieve small-worldness without sufficiently large constraints in the spatial domain for sparse networks compared to the exponential distribution (Kaiser and Hilgetag, 2004). The presence of long-range connections in the networks results in an overall reduction of average path length, but also impacts local clustering. This is due to the affinity for long-range connections resulting in a lower intermediate connectivity compared to the exponential system during network generation. Furthermore, the possibility of adding connections to just about any node in the system reduces the probability of a node connected distally to be connected to a second neighboring node, thereby reducing the clustering further. As such, the long-range connections have a negative effect on both small-worldness and modularity. Long-range connections come at the cost of local connections, with the nodes they connect to having a lower probability of making a connection to a neighbor in the local vicinity of the initial node. The exponential systems were more readily pushed into a small-world state, but in contrast to previous work, we found that sufficient spatial clustering was necessary also for this connection probability (Kaiser and Hilgetag, 2004; Onesto et al., 2017, 2019; Gentile, 2021).

Measuring the small-worldness of a network may give insight into the topology of the network, i.e. how the network balances local clustering with long range connections. Even so, a challenge of using this measure is the lack of standardization following the many ways of determining the small-worldness. Many of the metrics used to determine the small-worldness of a network have been criticized for shortcomings such as a dependence on both network size and density making comparison across studies challenging (Telesford et al., 2011; Neal, 2017). In the current study, we have opted for using the small-world propensity, which aims to improve on these challenges. The small-world

propensity has been shown to be more robust to choice of weights and less dependent on network density (Muldoon et al., 2016; Bassett and Bullmore, 2017). In our networks, increasing the number of connections did not improve small-worldness, further highlighting the importance of balancing connections within and beyond spatial clusters when considering computational capabilities of networks

Similarly to the increase in small-worldness, both the Q and Z modularity increases for increasing clustering. Overall the log-normal systems have lower modularity scores as compared to the exponential systems, but also separate into a larger number of communities, with the Z community number closely matching the expected cluster size, allowing for more finely tuned cluster sizes. These results suggest that the reduction in intermediate ranged connections result in segregation into more distinct communities, especially for Z modularity favoring the smaller community size. Even so, the overall modularity score is lower, suggesting that standard null models may not be able to capture the intricacies of spatially embedded models, and more representative modularity scores could be determined using null models for comparison better suited for the task for network comparison (Váša and Mišić, 2022).

As expected for geometric network models, we find that neither system were hierarchically structured (Ravasz and Barabási, 2003). This challenge of capturing hierarchical structures in networks of simple geometric dependencies may allude to secondary mechanisms being necessary for the formation of hierarchical networks. To capture such structures one option is to add additional steps to the model, such as the introduction of preferential attachment based on a given network characteristic (Holme and Kim, 2002; Gentile, 2021). Improving upon the model could capture both long-range and short-range interactions, all while allowing for the integration of hubs necessary for information transfer (Sporns et al., 2007; Meunier et al., 2010).

Through the use of simple geometric models for network generation we show that even a slight change in local connectivity with the introduction of long-range connections disrupts features considered important for computation in biological neural networks. Although such mechanisms may seem trivial, the apparent contradiction that the presence of long-range connections reduces small-worldness helps shed light onto mechanisms underlying disease or aging. In diseases such as amyotrophic lateral sclerosis, the networks in vitro have been shown to undergo alterations including increased neurite branching and reduced outgrowth (Akiyama et al., 2019; Garone et al., 2021). Analogous to our systems, an increase in neurite branching and local clustering combined with reduced long-range connections has been suggested to increase the overall small-worldness and modularity measures, resulting in reduced global efficiency (Rubinov and Sporns, 2010; Zhang et al., 2019). As we have previously shown, in networks subject to these maladaptive conditions such alterations can occur at different stages, ultimately affecting the activity of the networks (Kollstrøm et al., 2024; Valderhaug et al., 2024; Weir et al., 2023, 2024). Combined with spatial constraints in the distribution of nodes in the available area geometric network models may improve our understanding of how compensatory changes in regards to the formation and maintenance of connections at different ranges in neural networks shape onset of activity in different stages of disease.

In the current study, we limit our networks to sparse and binary networks when investigating the effects of clustering on network formation. On the contrary, biological neural networks have been shown to form dense networks (Ercsey-Ravasz et al., 2013; Rubinov et al., 2015), with weights often following a heavy tailed distribution (Antonello et al., 2022). Although we found that increasing the number of connections reduced small-worldness, the introduction of denser connectivity in combination with weights may increase biological plausibility and at the same time remain small-world (Bassett and Bullmore, 2017). Even though we focus our attention to sparse networks and do not include wights in our networks, we find the model to be representative for investigating the effects of long-range connections on network measures. The initial investigation of increasing network densities showed us that beyond a certain threshold, the choice of wiring probability functions were indistinguishable using a standard network analysis approach, emphasizing the importance on choice of model parameters.

Overall, we find that the adoption of geometric network models offer a simple and computationally efficient method for generating networks. Introducing length dependent weighting, such that the strength is inversely proportional with the length of the connection, replicating axon bundling through additional rewiring steps or adding branching along the connection projections, may increase the models ability to replicate processes related to neural networks. As such, these models allow for a wide range of tuning possibilities, with the extended possibility of adding additional steps to further their biological relevance, making it possible to study how different connection rules impact the resulting networks. This may allow for new insight into how the relation between neuron placement and simplified axon

growth rules change the resulting network properties, which may be of special interest in maladaptive conditions, such as disease.

Methods and Materials

Network generation. To generate networks two steps were performed. Firstly, nodes were assigned a position in a given space to act as a basis for the spatial embedding for each network. Secondly, nodes were connected through the adoption of a statistical wiring probability function. Two facets of interest were studied, namely how connections are recruited into the network for increasing network density for uniformly distributed nodes, and how network topology changes due to the introduction of spatial constraints and clustering for the spatial embedding.

Node placement. Nodes were placed on a Euclidean plane in a one-by-one unit square. The plane was embedded on a torus resulting in periodic boundary conditions. The use of periodic boundaries reduces the effects of finite sizes at the outer edges of the square and limits the inter-nodal distances to the range $[0,1)$.
The nodes were placed on the plane following either a uniform distribution of the nodes in the available area, or with nodes in clusters. In the case of the clustered distributions, an initial number of nodes (200, 100, 50 or 20) were uniformly distributed in the plane with subsequent nodes assigned an initial node. Allocation of nodes to a given cluster (i.e., initially placed node) was performed by uniformly distributing the remaining nodes among the initially placed nodes to ensure that assignment was random while clusters were kept at a comparable size.
The distances r from the initially placed nodes were chosen from a power law distribution determined by the equation

$$r = 4r_{min}(1-R)^{(-1/(\alpha-1))}, \tag{1}$$

where r_{min} is the radius of the node, R a random number in the range $[0,1)$ chosen from a uniform distribution, and α the power law exponent (Newman, 2005). The radius r_{min} was set to 10^{-4} to reflect neurons inability to occupy the same space, while α was chosen to be 1.5 to balance clustering around the initially placed nodes.
The radial direction of the nodes were chosen from a uniform distribution of angles in the range $[0,2\pi)$. In all cases, the position of each node was redrawn if the distance between any pair of nodes was less than $2r_{min}$ to avoid spatial overlap. To avoid overlapping clusters for the initially placed nodes in the clustered systems, $4r_{min}$ was used to reduce spatial overlap of subsequent clusters. Similarly, r_{min} in Equation 1 was multiplied by 4 to avoid excessive clustering at the central node. A total of 1000 nodes were placed in each system, and a total of 100 systems were generated for each conformation.
To ensure that streams of random numbers were not repeated, random numbers were handled according to the documentation using the Python package NumPy (Harris et al., 2020). A set of seeds were generated from an initial seed for each use case of random numbers. For each network, near independent seeds were generated to get unique streams of random numbers and avoid overlap.

Wiring probability functions determine connection probability by distance. Networks for each system were generated by connecting the nodes according to Waxman (1988). Whether or not an edge would occur between a given pair of nodes $\{u,v\}$ was determined by

$$P(\{u,v\}) - R > 0. \tag{2}$$

Here R is a random number in the range $[0,1)$ determined by a uniform distribution, and $P(\{u,v\})$ the probability function determining if a connection would be made. In Eq. 2, the wiring probability function $P(\{u,v\})$ is analogues to the wiring cost in neural networks, where the Euclidean distance $d_{\{u,v\}}$ between two nodes determines the probability that a connection would occur between a set of nodes.
To determine the connection probability, two separate wiring probability functions were used for each system, an exponential and a log-normal probability function respectively. For the exponential wiring probability function, $P(\{u,v\})$ was given by the equation

$$P(\{u,v\}) = \beta e^{\frac{-d_{\{u,v\}}}{\alpha L}}, \tag{3}$$

where α and β are tuning parameters, and L the largest calculated distance in the system.

In the case of the log-normal wiring probability, $P(\{u,v\})$ was given by

$$P(\{u,v\}) = \frac{1}{d_{\{u,v\}}\sigma\sqrt{2\pi}} e^{-\frac{1}{2}\left(\frac{\ln(d_{\{u,v\}}/L)-\mu}{\sigma}\right)^2}. \tag{4}$$

Again, μ and σ are tuning parameters used to determine the shape of the curve for the wiring probability, while L is defined similarly as in Eq. 3. By tuning the wiring probability functions, the number of connections made is changed. In both cases, the probability of establishing a connection decreases with increasing distance between nodes.
To investigate how connections were recruited into the network depending on the choice of wiring probability function for different connection degrees $\langle k \rangle$, the tuning parameters were manually chosen such that the mean degree, $\langle k \rangle$ was comparable between choices of wiring probability functions, with k ranging from 20 to 500. To study the effects of clustering on network formation, the tuning parameters were chosen such that k was comparable for both wiring probabilities for the uniform distribution and the resulting networks were sparse (i.e, $k_{max} \gg k$). For the latter case, α was set to 0.057 for the exponential wiring probability function and σ for the log-normal wiring probability was set to 65.4. For all simulations, β = 1 and μ = 0 were kept constant for their respective wiring probability function.

Network analysis. To classify the effects of changes to spatial distributions and choice of wiring probability function we calculated common network parameters.

Path length and network diameter. The average shortest path $\langle d \rangle$ is given by the average of all shortest paths, $d_{i,j}$, between all node pairs in the network,

$$\langle d \rangle = \frac{1}{n(n-1)} \sum_{i \neq j} d_{ij}. \tag{5}$$

The network diameter d_{max} is defined as the longest shortest path or maximum eccentricity. These measures indicate the average and largest numbers of steps necessary to traverse the network from one node to the next and the largest expected distance between two nodes.

Clustering coefficient. To measure how well connected locally the networks were we calculated the mean clustering coefficient $\langle C \rangle$ for each network, defined as

$$\langle C \rangle = \frac{1}{n} \sum_{i} c_i, \tag{6}$$

where n is the number of nodes in the network and c_i the clustering coefficient of the given node (Watts and Strogatz, 1998). The clustering of node i measures the number of connected neighbors indicating how many of the first degree connections of a given node are also connected connections.

Small-world propensity. A small-world organization is characterized by networks having both a high degree of clustering and short average path lengths, allowing for faster information transfer and propagation across the networks (Watts and Strogatz, 1998). To measure the affinity for the networks to organize into small-world structures we estimated the small-world propensity ϕ for each network according to Muldoon et al. (2016). ϕ is determined by

$$\phi = 1 - \sqrt{\frac{\Delta_C^2 + \Delta_L^2}{2}}, \tag{7}$$

where

$$\Delta_C = \frac{C_{latt} - C_{obs}}{C_{latt} - C_{rand}}, \tag{8}$$

and

$$\Delta_L = \frac{L_{obs} - L_{rand}}{L_{latt} - L_{rand}}. \tag{9}$$

Here, C_{obs} and L_{obs} are the mean clustering coefficient and average shortest path for the observed network, and C_{rand}, C_{latt}, L_{rand} and L_{latt} are the mean clustering coefficient and average shortest

path for equivalent (i.e. same number of nodes and vertices) random (*rand*) and lattice (*latt*) networks. A total of 100 random networks were generated to determine C_{rand} and L_{rand}, while the analytical C_{latt} and L_{latt} results for equivalent lattice networks, were used as references to determine Δ_C and Δ_L. The variables Δ_C and Δ_L are limited to the range $[0, 1]$, such that ϕ is constrained to the range $[0, 1]$. A ϕ of at least 0.6 is considered small-world.

Modular and hierarchical structures. To measure whether the networks segregated into subdivisions of densely connected modules (or communities), we calculated two separate modularity scores for each network. We first separated the network into modules using the Louvain method by varying the resolution parameter γ (Blondel et al., 2008). The resulting partitions were subsequently evaluated using either the Q or Z score for evaluating the modularity of the partitions (Newman and Girvan, 2004; Miyauchi and Kawase, 2016). For each respective modularity score we choose a range to iterate γ over in increments of 0.01. The modularity score was calculated 5 times for each increment to determine the γ value corresponding to the highest score for each respective metric in the chosen range. The final partitions were averaged over 50 repetitions for each network. For Q-modularity, γ was varied over the range$[0.5, 2]$, while the range $[5, 16]$ was used for evaluating the Z-modularity. When evaluating the Q-modularity a γ=1.0 was used.
To determine whether these networks were hierarchically structured we evaluated the dependence of the clustering of a given node on the degree according to Ravasz and Barabási (2003). This evaluation was performed by first pooling all networks with similar spatial distributions and wiring probability functions. For each value of k in the pooled groups, the clustering as a function of the degree, $C(k)$, was determined by taking the average of the clustering for all nodes with the same k. In hierarchical networks, $C(k)$ is expected to follow a power-law scaling, such that $C(k) \sim 1/k$.

Software. All simulations and subsequent analysis was performed using the Python programming language (Python Software Foundation, https://www.python.org/). Network parameters were analysed and determined using the Python packages NetworkX and CDlib (Hagberg et al., 2008; Rossetti et al., 2019). Data was processed using the Python package Pandas (Wes McKinney, 2010) and figures were generated using the Python packages Matplotlib and Seaborn (Hunter, 2007; Waskom, 2021).

FUNDING
This work was funded by ALS Norge.

AUTHOR CONTRIBUTIONS
NC: Conceptualization, Methodology, Software, Investigation, Formal Analysis, Visualization, Writing - Original Draft, Reviewing and Editing.
IS and AS: Conceptualization, Funding Acquisition, Project Administration, Supervision, and Writing — Review and Editing.

COMPETING FINANCIAL INTERESTS
The authors declare no competing interests.

References

Ahn, Y. Y., Jeong, H., and Kim, B. J. (2006). Wiring cost in the organization of a biological neuronal network. *Physica A: Statistical Mechanics and its Applications*, 367:531–537.

Akiyama, T., Suzuki, N., Ishikawa, M., Fujimori, K., Sone, T., Kawada, J., Funayama, R., Fujishima, F., Mitsuzawa, S., Ikeda, K., Ono, H., Shijo, T., Osana, S., Shirota, M., Nakagawa, T., Kitajima, Y., Nishiyama, A., Izumi, R., Morimoto, S., Okada, Y., Kamei, T., Nishida, M., Nogami, M., Kaneda, S., Ikeuchi, Y., Mitsuhashi, H., Nakayama, K., Fujii, T., Warita, H., Okano, H., and Aoki, M. (2019). Aberrant axon branching via Fos-B dysregulation in FUS-ALS motor neurons. *EBioMedicine*, 45:362–378.

Antonello, P. C., Varley, T. F., Beggs, J., Porcionatto, M., Sporns, O., and Faber, J. (2022). Self-organization of in vitro neuronal assemblies drives to complex network topology. *eLife*, 11.

Arvin, S., Glud, A. N., and Yonehara, K. (2022). Short- and Long-Range Connections Differentially Modulate the Dynamics and State of Small-World Networks. *Frontiers in Computational Neuroscience*, 15.

Avramiea, A. E., Masood, A., Mansvelder, H. D., and Linkenkaer-Hansen, K. (2022). Long-Range Amplitude Coupling Is Optimized for Brain Networks That Function at Criticality. *Journal of Neuroscience*, 42(11):2221–2233.

Barabási, A.-L., Albert, R., and Jeong, H. (1999). Mean-field theory for scale-free random networks. *Physica A: Statistical Mechanics and its Applications*, 272(1-2):173–187.

Bassett, D. S. and Bullmore, E. T. (2017). Small-World Brain Networks Revisited. *The Neuroscientist*, 23(5):499–516.

Beggs, J. M. (2008). The criticality hypothesis: How local cortical networks might optimize information processing. *Philosophical Transactions of the Royal Society A: Mathematical, Physical and Engineering Sciences*, 366(1864):329–343.

Betzel, R. F., Medaglia, J. D., Papadopoulos, L., Baum, G. L., Gur, R., Gur, R., Roalf, D., Satterthwaite, T. D., and Bassett, D. S. (2017). The modular organization of human anatomical brain networks: Accounting for the cost of wiring. *Network Neuroscience*, 1(1):42–68.

Blondel, V. D., Guillaume, J. L., Lambiotte, R., and Lefebvre, E. (2008). Fast unfolding of communities in large networks. *Journal of Statistical Mechanics: Theory and Experiment*, 2008(10).

Bullmore, E. and Sporns, O. (2012). The economy of brain network organization. *Nature Reviews Neuroscience*, 13(5):336–349.

Chen, B. L., Hall, D. H., and Chklovskii, D. B. (2006). Wiring optimization can relate neuronal structure and function. *Proceedings of the National Academy of Sciences of the United States of America*, 103(12):4723–4728.

Cherniak, C. (1994). Component placement optimization in the brain. *Journal of Neuroscience*, 14(4):2418–2427.

Ercsey-Ravasz, M., Markov, N. T., Lamy, C., VanEssen, D. C., Knoblauch, K., Toroczkai, Z., and Kennedy, H. (2013). A Predictive Network Model of Cerebral Cortical Connectivity Based on a Distance Rule. *Neuron*, 80(1):184–197.

Erdos, P., Rényi, A., et al. (1960). On the evolution of random graphs. *Publ. Math. Inst. Hung. Acad. Sci*, 5(1):17–60.

Garone, M. G., Birsa, N., Rosito, M., Salaris, F., Mochi, M., de Turris, V., Nair, R. R., Cunningham, T. J., Fisher, E. M., Morlando, M., Fratta, P., and Rosa, A. (2021). ALS-related FUS mutations alter axon growth in motoneurons and affect HuD/ELAVL4 and FMRP activity. *Communications Biology*, 4(1).

Gentile, F. (2021). Multipoint connection by long-range density interaction and shortrange distance rule. *Physica Scripta*, 96(4).
Gentile, F. (2024). The free energy landscape of small-world networks of cells. *Journal of Biomechanics*, 162.
Goulas, A., Betzel, R. F., and Hilgetag, C. C. (2019). Spatiotemporal ontogeny of brain wiring. *Science Advances*, 5(6).
Hagberg, A. A., Schult, D. A., and Swart, P. J. (2008). Exploring network structure, dynamics, and function using networkx. In Varoquaux, G., Vaught, T., and Millman, J., editors, *Proceedings of the 7th Python in Science Conference*, pages 11 – 15, Pasadena, CA USA.
Harris, C. R., Millman, K. J., van der Walt, S. J., Gommers, R., Virtanen, P., Cournapeau, D., Wieser, E., Taylor, J., Berg, S., Smith, N. J., Kern, R., Picus, M., Hoyer, S., van Kerkwijk, M. H., Brett, M., Haldane, A., del Río, J. F., Wiebe, M., Peterson, P., Gérard-Marchant, P., Sheppard, K., Reddy, T., Weckesser, W., Abbasi, H., Gohlke, C., and Oliphant, T. E. (2020). Array programming with NumPy. *Nature*, 585(7825):357–362.
Hayward, C. J., Huo, S., Chen, X., and Kaiser, M. (2023). Nonoptimal component placement of the human connectome supports variable brain dynamics. *Network Neuroscience*, 7(1):254–268.
Holme, P. and Kim, B. J. (2002). Growing scale-free networks with tunable clustering. *Physical Review E - Statistical Physics, Plasmas, Fluids, and Related Interdisciplinary Topics*, 65(2).
Hunter, J. D. (2007). Matplotlib: A 2d graphics environment. *Computing in Science & Engineering*, 9(3):90–95.
Kaiser, M. (2010). Hierarchy and dynamics of neural networks. *Frontiers in Neuroinformatics*, 4(AUG).
Kaiser, M. and Hilgetag, C. C. (2004). Spatial growth of real-world networks. *Physical Review E - Statistical, Nonlinear, and Soft Matter Physics*, 69(3 2).
Kaiser, M. and Hilgetag, C. C. (2006). Nonoptimal component placement, but short processing paths, due to long-distance projections in neural systems. *PLoS Computational Biology*, 2(7):0805–0815.
Khambhati, A. N., Sizemore, A. E., Betzel, R. F., and Bassett, D. S. (2018). Modeling and interpreting mesoscale network dynamics. *NeuroImage*, 180:337–349.
Klemm, K. and Eguíluz, V. M. (2002). Growing scale-free networks with small-world behavior. *Physical Review E - Statistical, Nonlinear, and Soft Matter Physics*, 65(5).
Kollstrøm, A. M., Christiansen, N., Sandvig, A., and Sandvig, I. (2024). Dysregulation of synaptic transcripts underlies network abnormalities in ALS patient-derived motor neurons. *bioRxiv*.
Laughlin, S. B. (2003). Communication in Neuronal Networks. *Science*, 301(5641):1870–1874.
Markov, N. T., Ercsey-Ravasz, M., Lamy, C., Gomes, A. R. R., Magrou, L., Misery, P., Giroud, P., Barone, P., Dehay, C., Toroczkai, Z., Knoblauch, K., Van Essen, D. C., and Kennedy, H. (2013). The role of long-range connections on the specificity of the macaque interareal cortical network. *Proceedings of the National Academy of Sciences of the United States of America*, 110(13):5187–5192.
Massobrio, P., Pasquale, V., and Martinoia, S. (2015). Self-organized criticality in cortical assemblies occurs in concurrent scale-free and small-world networks. *Scientific Reports*.
Meunier, D., Lambiotte, R., and Bullmore, E. T. (2010). Modular and Hierarchically Modular Organization of Brain Networks. *Frontiers in Neuroscience*, 4(DEC).
Miyauchi, A. and Kawase, Y. (2016). Z-score-based modularity for community detection in networks. *PLoS ONE*, 11(1).
Muldoon, S. F., Bridgeford, E. W., and Bassett, D. S. (2016). Small-world propensity and weighted brain networks. *Scientific Reports*, 6.
Neal, Z. P. (2017). How small is it? Comparing indices of small worldliness. *Network Science*, 5(1):30–44.
Newman, M. E. (2005). Power laws, Pareto distributions and Zipf's law. *Contemporary Physics*, 46(5):323–351.
Newman, M. E. and Girvan, M. (2004). Finding and evaluating community structure in networks. *Physical Review E - Statistical, Nonlinear, and Soft Matter Physics*, 69(2 2):1–15.
Okujeni, S. and Egert, U. (2019a). Inhomogeneities in Network Structure and Excitability Govern Initiation and Propagation of Spontaneous Burst Activity. *Frontiers in Neuroscience*, 13(May):1–14.
Okujeni, S. and Egert, U. (2019b). Self-organization of modular network architecture by activity-dependent neuronal migration and outgrowth. *eLife*, 8:1–29.
Okujeni, S., Kandler, S., and Egert, U. (2017). Mesoscale Architecture Shapes Initiation and Richness of Spontaneous Network Activity. *The Journal of Neuroscience*, 37(14):3972–3987.
Onesto, M. M., Short, C. A., Rempel, S. K., Catlett, T. S., and Gomez, T. M. (2021). Growth Factors as Axon Guidance Molecules: Lessons From in vitro Studies. *Frontiers in Neuroscience*, 15.
Onesto, V., Cancedda, L., Coluccio, M. L., Nanni, M., Pesce, M., Malara, N., Cesarelli, M., DI Fabrizio, E., Amato, F., and Gentile, F. (2017). Nano-topography Enhances Communication in Neural Cells Networks. *Scientific Reports*, 7(1):1–18.
Onesto, V., Romano, M., Gentile, F., and Amato, F. (2019). Relating the small world coefficient to the entropy of 2D networks and applications in neuromorphic engineering. *Journal of Physics Communications*, 3(9).
Pan, R. K. and Sinha, S. (2007). Modular networks emerge from multiconstraint optimization. *Physical Review E - Statistical, Nonlinear, and Soft Matter Physics*, 76(4).
Ravasz, E. and Barabási, A. L. (2003). Hierarchical organization in complex networks. *Physical Review E - Statistical Physics, Plasmas, Fluids, and Related Interdisciplinary Topics*, 67(2):7.
Rossetti, G., Milli, L., and Cazabet, R. (2019). Cdlib: a python library to extract, compare and evaluate communities from complex networks. *Applied Network Science*, 4(1):1–26.
Rubinov, M. and Sporns, O. (2010). Complex network measures of brain connectivity: Uses and interpretations. *NeuroImage*, 52(3):1059–1069.
Rubinov, M., Ypma, R. J., Watson, C., Bullmore, E. T., and Raichle, M. E. (2015). Wiring cost and topological participation of the mouse brain connectome. *Proceedings of the National Academy of Sciences of the United States of America*, 112(32):10032–10037.
Sporns, O., Honey, C. J., and Kötter, R. (2007). Identification and classification of hubs in brain networks. *PLoS ONE*, 2(10).
Telesford, Q. K., Joyce, K. E., Hayasaka, S., Burdette, J. H., and Laurienti, P. J. (2011). The Ubiquity of Small-World Networks. *Brain Connectivity*, 1(5):367–375.
Valderhaug, V. D., Ramstad, O. H., van de Wijdeven, R., Heiney, K., Nichele, S., Sandvig, A., and Sandvig, I. (2024). Micro-and mesoscale aspects of neurodegeneration in engineered human neural networks carrying the LRRK2 G2019S mutation. *Frontiers in Cellular Neuroscience*, 18.
Váša, F. and Mišić, B. (2022). Null models in network neuroscience. *Nature Reviews Neuroscience*, 23(8):493–504.
Waskom, M. L. (2021). seaborn: statistical data visualization. *Journal of Open Source Software*, 6(60):3021.
Watts, D. J. and Strogatz, S. H. (1998). Collective dynamics of 'small-world' networks. *Nature*, 393(6684):440–442.
Waxman, B. M. (1988). Routing of Multipoint Connections. *IEEE Journal on Selected Areas in Communications*, 6(9):1617–1622.
Weir, J. S., Hanssen, K. S., Winter-Hjelm, N., Sandvig, A., and Sandvig, I. (2024). Evolving alterations of structural organization and functional connectivity in feedforward neural networks after induced P301L tau mutation. *bioRxiv*, page 2023.09.12.557339.
Weir, J. S., Huse Ramstad, O., Sandvig, A., and Sandvig, I. (2023). Inhibition of excitatory synaptic transmission alters functional organization and efficiency in cortical neural networks. *bioRxiv*, page 2023.07.05.547785.
Wes McKinney (2010). Data Structures for Statistical Computing in Python. In Stéfan van der Walt and Jarrod Millman, editors, *Proceedings of the 9th Python in Science Conference*, pages 56 – 61.
Yamamoto, H., Moriya, S., Ide, K., Hayakawa, T., Akima, H., Sato, S., Kubota, S., Tanii, T., Niwano, M., Teller, S., Soriano, J., and Hirano-Iwata, A. (2018). Impact of modular organization on dynamical richness in cortical networks. *Science Advances*, 4(11).
Yamamoto, H., Spitzner, F. P., Takemuro, T., Buendía, V., Murota, H., Morante, C., Konno, T., Sato, S., Hirano-Iwata, A., Levina, A., Priesemann, V., Muñoz, M. A., Zierenberg, J., and Soriano, J. (2023). Modular architecture facilitates noise-driven control of synchrony in neuronal networks. *Science Advances*, 9(34).
Zhang, Y., Qiu, T., Yuan, X., Zhang, J., Wang, Y., Zhang, N., Zhou, C., Luo, C., and Zhang, J. (2019). Abnormal topological organization of structural covariance networks in amyotrophic lateral sclerosis. *NeuroImage: Clinical*, 21:101619.

Supplementary Note A: Probability density functions

Dependence on the distance on the probability density functions of a connection occurring (A.1). The distance used is the normalized distance in the range [0.001, 1]. Both probabilities for making connections are large for $d < 0.01$. Beyond this the log-normal connection probability decreases fast but maintains a heavy-tail, whereas the exponential probability shows a preference for intermediate ranges up to $d < 0.2$, beyond which the probability declines fast.

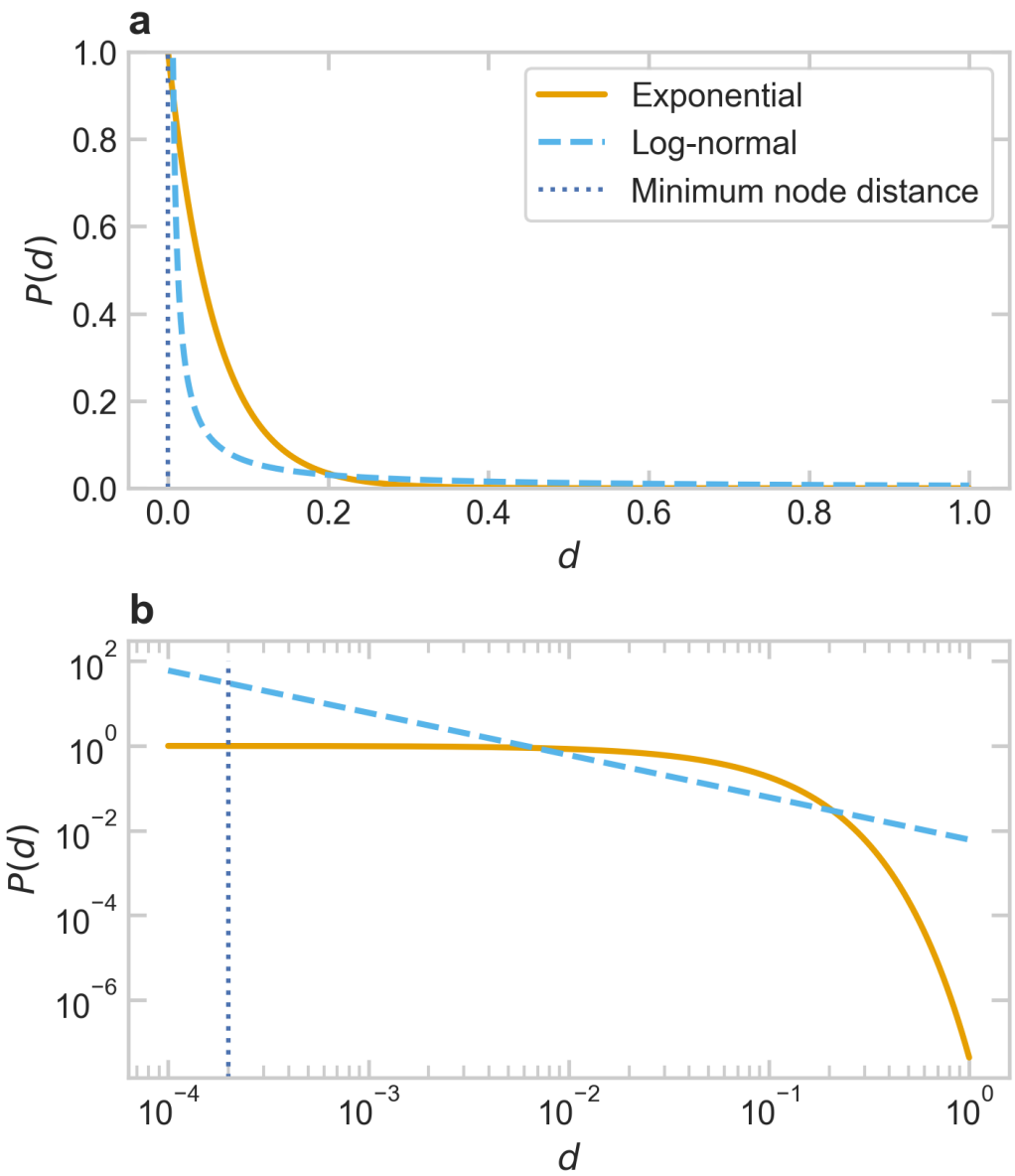

Fig. A.1. Probability density function $P(d)$ of a connection being made between two nodes as a function of the distance d. **(a)** Probability density function $P(d)$ of finding a connection at a distance d for the exponential and log-normal connection probabilities. **(b)** Same $P(d)$ as in **(a)** on a log-log scale. The vertical dotted line indicates the shortest distance between two nodes allowed in the systems. For the exponential probability $\alpha = 0.059$ and $\beta = 1$, while $\sigma = 65.4$ and $\mu = 0$ in the log-normal case. Legends shared between figures.

Supplementary Note B: Network parameters for increased network density

To determine the effect of increased connectivity in the network, the probability functions determining the connection probabilities were tuned such that $\langle k \rangle \approx 100$ for the uniform systems.

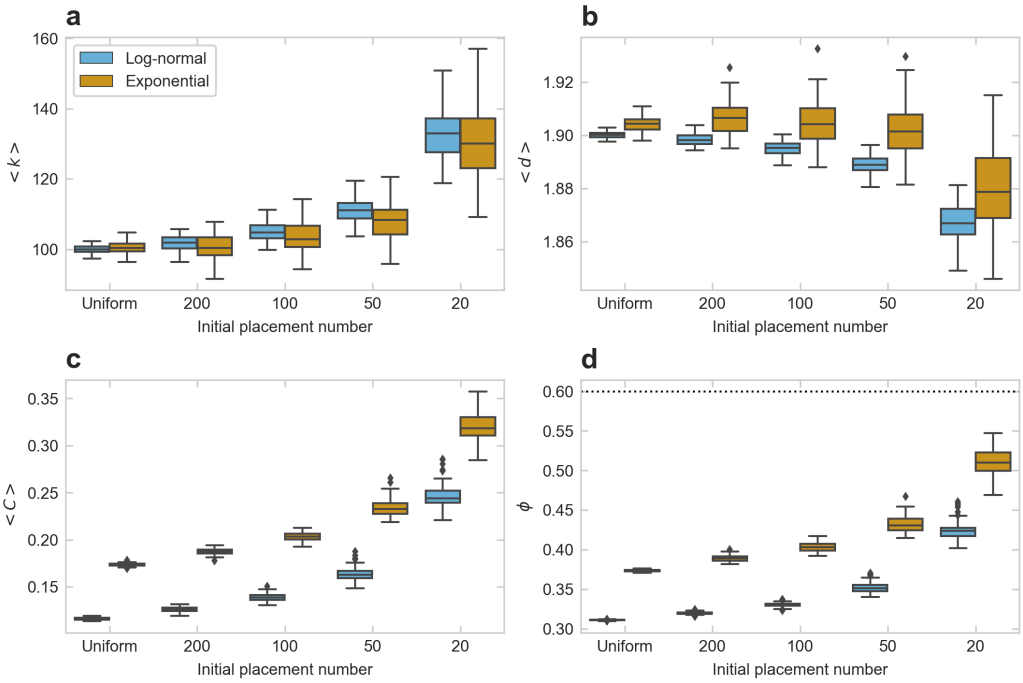

Fig. B.1. Parameters describing common network characteristics for networks tuned to have a mean degree of 100 for the uniform distribution. **(a)** Average degree, $\langle k \rangle$, **(b)** average shortest distance, $\langle d \rangle$, **(c)** mean local clustering, $\langle C \rangle$ and **(d)** small-world propensity, ϕ, for the uniform node placement and increasing cluster size. Each box plot represents the values for 100 realizations of each configuration. Legends shared between figures. Outliers denoted with diamonds.